Low probability of detection underwater acoustic communications using direct-sequence spread spectrum

T. C. Yang[a)]
Naval Research Laboratory, Washington, DC 20375

Wen-Bin Yang
National Institute of Standards and Technology, Gaithersburg, Maryland 20899

(Received 23 May 2008; revised 3 September 2008; accepted 4 September 2008)

Direct-sequence spread spectrum is used for underwater acoustic communications between nodes, at least one of which is moving. At-sea data show that the phase change due to source motion is significant: The differential phase between two adjacent symbols is often larger than the phase difference between symbols. This poses a challenge to phase-detection based receiver algorithms when the source or receiver is moving. A pair of energy detectors that are insensitive to the phase fluctuations is proposed, whose outputs are used to determine the relationship between adjacent symbols. Good performance is achieved for a signal-to-noise ratio (SNR) as low as −10 dB based on at-sea data. While the method can be applied to signaling using short code sequences, the focus in this paper is on long code sequences for the purpose of achieving a high processing gain (at the expense of a low data rate), so that communications can be carried out at a low input SNR to minimize the probability of detection (P_D) by an interceptor. P_D is calculated for a typical shallow water environment as a function of range for several source levels assuming a broadband energy detector with a known signal bandwidth. [DOI: 10.1121/1.2996329]

PACS number(s): 43.60.Dh [EJS] Pages: 3632–3647

I. INTRODUCTION

Direct-sequence spread-spectrum (DSSS) signaling uses phase coherent signals where the information symbols are multiplied with a code sequence, commonly known as chips.[1] The signals are processed at the receiver using the code sequence as a matched filter to extract the information symbols.[1–3] Taking advantage of the processing gain derived from the matched filter, communications can be carried out at low signal levels (e.g., below the noise level) to avoid detection and interception by an unfriendly party. This paper examines the probability of detection and counterdetection range for DSSS signaling in an underwater acoustic environment for acoustic communications involving mobile platforms. As is expected, the probability of detection, as well as the probability of interception, is very much dependent on the input signal-to-noise ratio (SNR) at the interceptor[4,5] and the recognition differential of the signal waveform. The fact that a low level source can be used for DSSS communications and that the signal is noiselike presents certain advantages from the point of view of low probability of detection (LPD). This topic will be analyzed later in this paper.

The problem for DSSS communications in an underwater acoustic channel is the multipath arrivals, which create severe interchip and intersymbol interferences. Decision feedback equalizer (DFE) and Rake receiver have been adapted for DSSS communications.[6,7] To achieve precise symbol synchronization and channel equalization, high SNR signals are required.[8] Recently, Yang and Yang[9,10] have demonstrated two new approaches for low input-SNR DSSS communications in a dynamic ocean environment between fixed nodes. Minimal (<1%) bit error rate (BER) can be achieved for in-band SNR as low as −11 to −14 dB. Signal phase distortion due to signal propagation in a random medium, achievable matched-filter gain (the ratio of output signal level to input signal level), and achievable processing gain (the ratio of output SNR to input SNR) were measured from data. Performance degradation of the receiver algorithm due to coarse synchronization at low input SNRs, signal fading, and imprecise knowledge of the channel were modeled and compared with data.

The DSSS signaling method uses code "orthogonality" to minimize interference between symbols. The code orthogonality requires that the code sequence is almost orthogonal to any of the cyclically shifted code sequences. With orthogonality, the matched-filter output yields a low sidelobe level and thus ensures minimum interference in a simple environment (dominated by a single path). It assures accurate symbol synchronization. The phase of the matched-filter output can then be used to determine the symbol sequence. In an underwater acoustic channel containing many multipath arrivals, the code orthogonality is severely degraded resulting in interchip interference. The phase is often path dependent and changing rapidly with time. At-sea data showed that the symbol phase error estimated from the matched-filter output is often larger than the phase difference between the symbols, resulting in unacceptable bit errors even with a high input SNR.[9,10] The challenge is to develop a receiver algorithm, patterned after the simple DSSS signal processing mentioned above, without employing a DFE to equalize the multipath arrivals, and a phase-locked loop (PLL) to remove/compensate the phase fluctuations in a dy-

[a)]Electronic mail: yang@wave.nrl.navy.mil

Report Documentation Page

Form Approved
OMB No. 0704-0188

1. REPORT DATE	2. REPORT TYPE	3. DATES COVERED
03 SEP 2008		**00-00-2008 to 00-00-2008**

4. TITLE AND SUBTITLE	5a. CONTRACT NUMBER
Low probability of detection underwater acoustic communications using direct-sequence spread spectrum	5b. GRANT NUMBER
	5c. PROGRAM ELEMENT NUMBER
6. AUTHOR(S)	5d. PROJECT NUMBER
	5e. TASK NUMBER
	5f. WORK UNIT NUMBER
7. PERFORMING ORGANIZATION NAME(S) AND ADDRESS(ES) **Naval Research Laboratory,Washington,DC,20375**	8. PERFORMING ORGANIZATION REPORT NUMBER
9. SPONSORING/MONITORING AGENCY NAME(S) AND ADDRESS(ES)	10. SPONSOR/MONITOR'S ACRONYM(S)
	11. SPONSOR/MONITOR'S REPORT NUMBER(S)

12. DISTRIBUTION/AVAILABILITY STATEMENT
Approved for public release; distribution unlimited

13. SUPPLEMENTARY NOTES

14. ABSTRACT

15. SUBJECT TERMS

16. SECURITY CLASSIFICATION OF:			17. LIMITATION OF ABSTRACT	18. NUMBER OF PAGES	19a. NAME OF RESPONSIBLE PERSON
a. REPORT **unclassified**	b. ABSTRACT **unclassified**	c. THIS PAGE **unclassified**	**Same as Report (SAR)**	**16**	

namic ocean. Toward this goal, a second layer of correlator, which cross-correlates the matched-filter outputs of two adjacent symbols, was implemented by Yang and Yang,[9,10] to estimate their differential phase. This method requires only "coarse" synchronization at the symbol level and is applicable to low input-SNR communications between fixed nodes.

In practice, underwater acoustic communications often involve mobile platforms. For DSSS signaling, Doppler shift, if not corrected for, destroys the orthogonality of the code sequences between the replica signal and data, and between code sequences of different users. In addition, the signal coherence time is significantly reduced due to the source/receiver motion.[11] The reason is traced to the rapidly fluctuating (relative) phases of the multipaths. As a symbol phase is determined by interference between the multipaths, medium fluctuation causes a symbol phase to change with time. For a moving source, the individual paths encounter, in addition, a different phase change (ray path-length change) due to source changing range. A higher rate of phase fluctuation is thus expected, resulting in a shorter coherence time for a moving source than for a fixed source. One finds[9,10] for a fixed source/receiver pair that while the phase of individual symbols changes rapidly with time, the differential phase between the symbols is relatively small. In contrast, the analysis below will show that, for the moving-source data, after proper Doppler compensation, the differential phase between symbols changes rapidly with time, and is often larger than the phase difference between true symbols even with a high input SNR. Hence, while differential phase shift keying (DPSK) can be used to decode the signal for the fixed-source data, this method (based on the differential phase) is expected to encounter high bit errors when applied to the moving-source data.

For DSSS signaling involving a mobile platform, a new method, which is insensitive to the phase fluctuation, is developed in this paper and applied to at-sea data. This method can also be applied to fixed-source data. It will be shown below that the method, applied to the fixed-source data reported previously, yields a slightly degraded, but still satisfactory, performance compared with the method mentioned above.

Like the cross-correlation method, the new method can be applied to DSSS signals with short or long code sequences so long as the code length is longer than the multipath spread. Similar to the previous work,[9,10] the focus of this paper is on communications with a long code sequence for the purpose of LPD. A long sequence yields a high processing gain, which allows communications using a low source level (SL), thus minimizing the probability of detection by a hostile party.[9,10] For a given bandwidth, longer sequences imply lower data rates. One can increase the data rate through other means, such as spreading the data over multiple orthogonal codes at the price of a slightly higher SL. That topic is beyond the scope of this paper.

This paper is organized as follows: In Sec. II the characteristics of a signal emitted from a moving source are analyzed, including the fluctuation of the Doppler shift found in the data. In Sec. III, the phase insensitive method is presented, tested against the fixed-source data, and then applied to the moving-source data. In Sec. IV, the probability of detection and the probability of false alarm are analyzed for an energy detector assuming the interceptor has no knowledge of the signal waveform and signal parameter. The ability to communicate with a lower SL using the DSSS signaling is shown to significantly reduce the probability of detection by an interceptor.

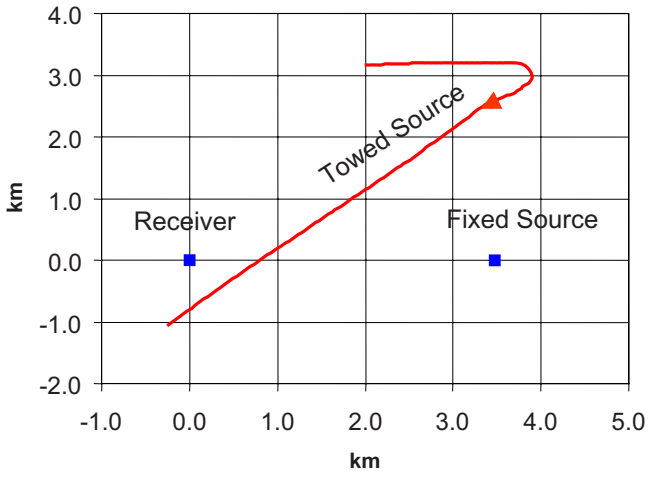

FIG. 1. (Color online) Source-receiver geometry including the towed source run.

Regarding LPD underwater acoustic communications, a simple system concept may be helpful to motivate and guide the analysis below. A potential scenario for LPD communications will be cooperative operation between autonomous underwater vehicles (AUVs), which stay together within a certain range from each other and use LPD acoustic communications to avoid detection by a nearby interceptor. From the system point of view, the SL needs to be high enough to assure reliable communications with neighboring AUVs, and yet low enough so not to alert the interceptor of their presence. The question is at what range will the detection (by the interceptor) become unavoidable, i.e., the counterdetection range. Counterdetection range is calculated in Sec. IV for a typical shallow water environment assuming certain system parameters.

II. SIGNAL CHARACTERISTICS

The data were taken during the TREX04 (time reversal experiment) conducted by the Naval Research Laboratory in April 2004, off the coast of New Jersey, southwest of the Hudson Canyon. The sound speed profile presented a minimum in the middle of the water column (see Fig. 1, Ref. 10). Acoustic communication data were transmitted from a fixed source to a fixed-receiver array at the range of 3.4 km, and from a towed source to the fixed receiver as shown in Fig. 1. The water depth in the experimental area is about 70 m. The fixed source and receivers were located at about 35 m depth. The towed source was at a depth of approximately 20 m. The vertical array has an aperture of approximately 2 m and contains eight hydrophones with nonuniform spacing. Only one receiver is used for communications from the fixed and towed sources.

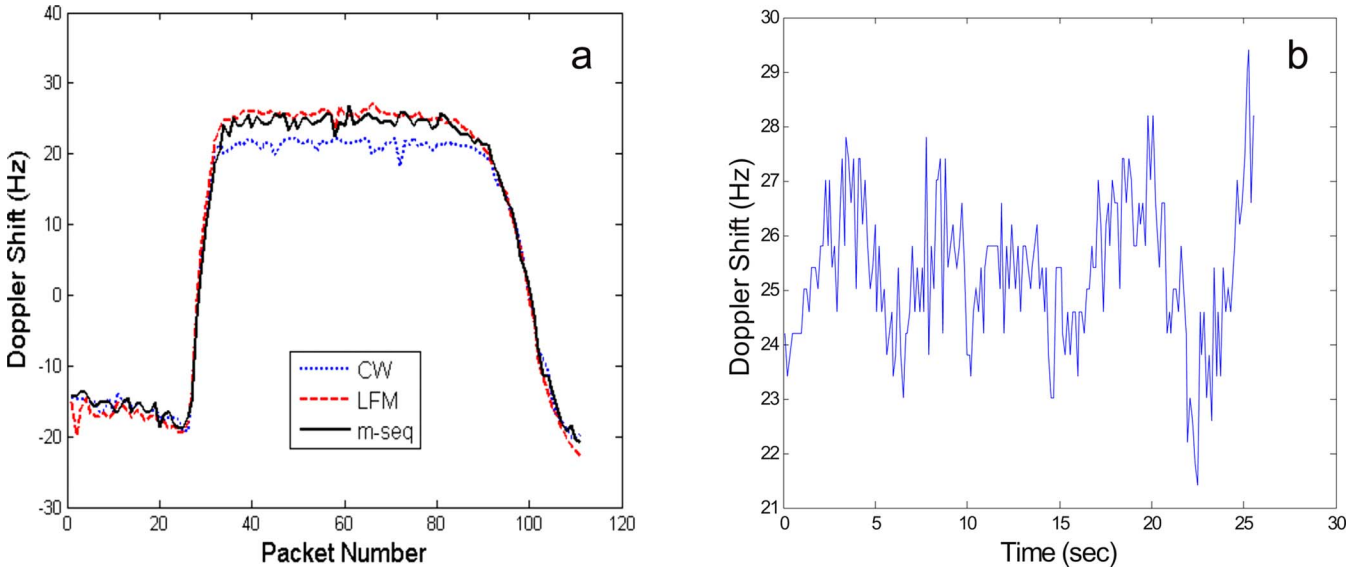

FIG. 2. (Color online) Estimation of the mean Doppler shift over a packet as a function of packet number using different signals (a). Instantaneous Doppler shift within a packet based on *m*-sequence ambiguity function (b).

The DSSS signals were centered at 17 kHz and had a bandwidth of 4 kHz. The transmitted symbols were spread with (multiplied by) an *m*-sequence containing 511 chips yielding a theoretical processing gain of 27 dB at the receiver. The sequence of chips coded with the message data was then transmitted using binary phase-shift-keying modulation. Each symbol has a duration of 127.8 ms, yielding a data rate of ~8 bits/s. So long as the symbol duration is longer than the multipath spread, the interference between adjacent symbols is minimal. [For example, see Fig. 1(b) of Ref. 10.] Each packet contains 200 symbols lasting approximately 25.55 s. A total of 111 packets were transmitted over approximately an hour. The signal properties are discussed in this section. BERs are reported in the next section.

In this experiment, some auxiliary signals, such as pilot tones and linear frequency modulation (LFM) signals, were added to each packet for independent probing of the channel properties. Pilot tones signals shall not be used for DSSS communications at a low SNR. Data acquisition and symbol synchronization can be done by matched filtering the data with the LFM or *m*-sequence replicas.[9,10]

A. Doppler shift

A key feature of the moving-source data is the Doppler shift/spread. The Doppler shift is path dependent as multipaths arrive with different depression/elevation (D/E) angles. At long ranges, the multipaths are confined to shallow ($<10°$) D/E angles as deep D/E angle paths are attenuated by the bottom. Under these conditions, one can assume the same Doppler shift for all the paths. At short ranges, both shallow and deep rays exist. As a result, the path-dependent Doppler shifts create a (large) Doppler spread. Note that an individual path may also have a Doppler spread due to scattering with ocean medium and/or surface. The path-dependent Doppler spread, most notable at short ranges, can be (much) larger than the medium/boundary induced Doppler spread.

The first task in the data analysis is Doppler estimation as the data have to be corrected for the Doppler shift.[12] The temporal variation of the Doppler shift on the scale of the order of a minute can be obtained by measuring the average Doppler shift for each packet. Three methods are used to estimate the average Doppler shift. The first method determines the average Doppler shift from the pilot tones, which were placed above and below the DSSS signal band. The result is shown as the dotted line in Fig. 2(a). The second method determines the average Doppler shift from the time separation between the two LFM signals placed before and after the data packet measured against that of the transmitted signal. The measured Doppler shift is shown as the dashed line in Fig. 2(a). The third method measures the Doppler shift from each *m*-sequence. The input data are bandpass filtered and shifted to the base band. The base band data are synchronized and partitioned into (overlaying) blocks, each containing one *m*-sequence. A wideband ambiguity function is created for each block of data by correlating the data with a Doppler-shifted transmitted *m*-sequence signal. The output is an impulse response as a function of Doppler shift and delay time, referred to as the ambiguity function. The peak of the ambiguity surface determines the Doppler shift for the data block. The measured Doppler shift as a function of the block (or sequence) number is shown in Fig. 2(b) using one packet of data as an example. The Doppler shift is averaged for each packet, and the result is shown in Fig. 2(a) by the solid line as a function of packet number.

Based on the source track in Fig. 1, the source moved out initially by an opening range. It turned around at a range about 5 km and moved toward the receiver; it reached a closest point of approach near the end of the run. [The source-receiver range is shown in Fig. 3(a) as a function of the packet number.] One thus expects initially a negative Doppler shift, which should change into a positive Doppler shift and then crosses over into a negative Doppler shift again. This is in accord with the measured Doppler shift. One finds

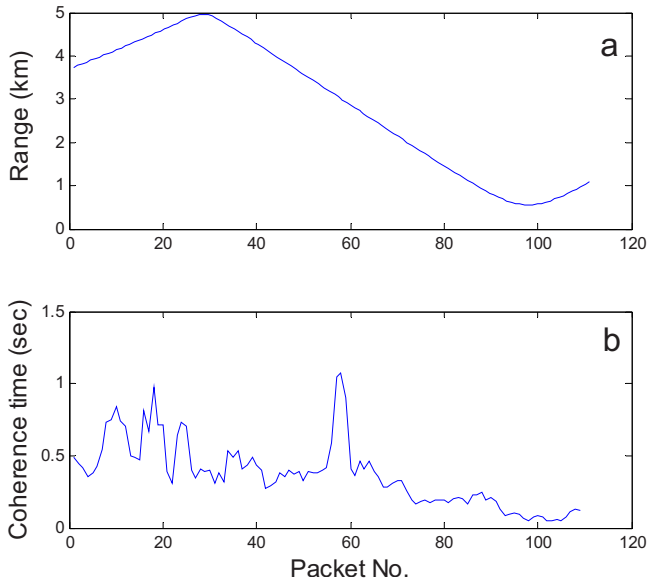

FIG. 3. (Color online) Source-receiver range as a function of time (packet number) (a). Signal coherence time as a function of time (packet number) (b).

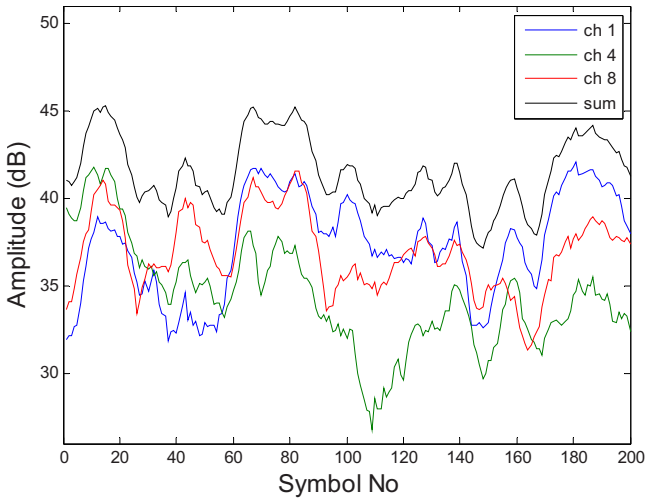

FIG. 4. (Color online) Signal amplitude as a function of time within a packet for three selected receivers.

that the Doppler shift measured from the LFM and *m*-sequence signals agree relatively well with each other. The measurement using the pilot tones is somewhat (a few hertz) lower than using LFM and *m*-sequence. The reason is the ambiguity in the spectral determination of the Doppler shift. Using the spectral analysis, an integration time of 2 s is required, for example, to achieve a Doppler resolution of 0.5 Hz. However, during the 2 s period, the Doppler shift changes with time as shown next.

Figure 2(b) shows the Doppler shift within a packet. One may expect the Doppler shift to vary slowly with time [based on Fig. 2(a)], and be surprised that the Doppler shift varies by 3–5 Hz with a period of 4–7 s. This variation is attributed to the heave motion of the ship, which was observed during the experiment, and expected to cause the tow body to speed up and down with the ship motion. For data processing, what is significant is that the Doppler shift varies from symbol to symbol [Fig. 2(b)]; each symbol is ~128 ms long. This requires the Doppler shift to be estimated for every symbol, which increases significantly the data processing load.

B. Temporal coherence: Signal coherence time

The Doppler corrected impulse responses are used to estimate the temporal coherence of the *m*-sequence signals as defined by

$$\rho(\tau) = \frac{[p^*(t)p(t+\tau)]}{\sqrt{[p^*(t)p(t)][p^*(t+\tau)p(t+\tau)]}}, \quad (1)$$

where $p(t)$ and $p(t+\tau)$ are the impulse responses of the two consecutive *m*-sequences separated by a lag time τ; t is the sample time of the impulse response. The square bracket $[ab]$ denotes the maximum absolute value of the correlation between $a(t)$ and $b(t)$. (For the measurement of the impulse response and temporal coherence using *m*-sequences, the reader is referred to Ref. 13.) The signal coherence time $\tau_{0.8}$ is defined as the lag time when the coherence value drops from 1 to 0.8. Temporal coherence of the *m*-sequence signal is measured for each packet and the measured signal coherence time is shown as a function of packet number in Fig. 3(b).

One finds in Fig. 3(b) that the signal coherence time at close ranges (<1 km) is ~0.1 s compared with the signal coherence time at 3 km, which is of the order of 0.5 s. Note that the signal coherence time is inversely proportional to the signal Doppler spread. At close ranges, the multipaths have different Doppler shifts, resulting in a decreased coherence time. Later in Sec. III, it will be shown that the "large" Doppler spread presents a problem for Doppler compensation and is responsible for degraded BER performance at close ranges.

C. Signal-fading statistics

Figure 4 shows an example of the time variation of the symbol amplitude using one packet of data. The amplitude variation is shown for three receivers spaced by approximately 0.3 m, as well as the amplitude of the linear sum of the pressure fields on all eight receivers. Fading by as much as 10–20 dB is seen in the data. Since detection performance is affected by signal fading, one needs to examine the signal-fading statistics for a moving source (on a single receiver). For amplitude statistics, the amplitude is estimated from the square root of the symbol energy, conventionally denoted as E_b. Figure 5(a) shows the symbol amplitude distribution at a fixed range of 3.4 km (Fig. 10 of Ref. 10). It was found consistent with a log-normal distribution

$$p(s) = \frac{1}{\sqrt{2\pi}\sigma_s} s^{-1} \exp\left(-\frac{(\ln s - \mu_s)^2}{2\sigma_s^2}\right), \quad (2)$$

where s is the signal amplitude; $s>0$. The mean and variance of the signal amplitude are expressed in terms of two parameters, μ_s and σ_s, as follows:

$$m_s = \exp(\mu_s + \sigma_s^2/2),$$

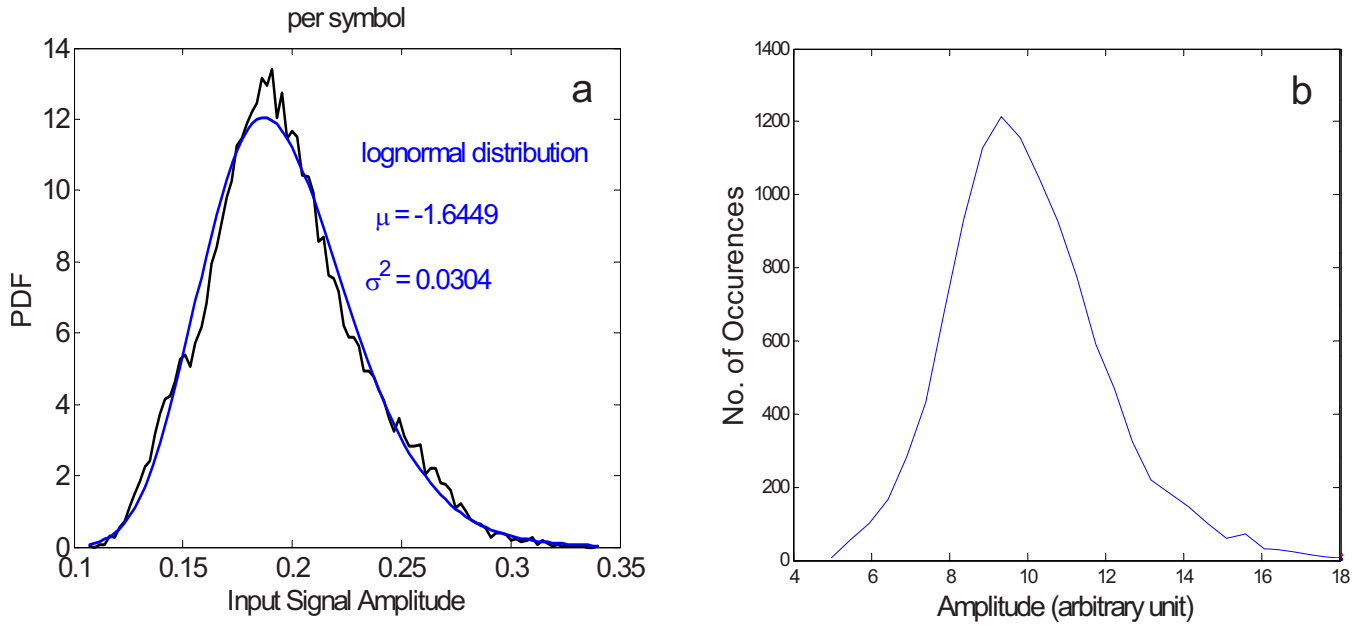

FIG. 5. (Color online) Probability distribution of signal amplitude for fixed-source data compared with the log-normal distribution (a) and histogram distribution of signal amplitude from the moving-source data (b).

$$v_s^2 = \exp(2\mu_s + \sigma_s^2)[\exp(\sigma_s^2) - 1].$$

The data were fitted in Fig. 5(a) using $\mu_s = -1.6449$ and $\sigma_s^2 = 0.0304$; the corresponding mean signal level and its variance are $m_s = 0.196$ and $v_s^2 = 1.186 \times 10^{-3}$.

One can generalize Eq. (2) to model the data from a moving source, such as communication data from an autonomous underwater vehicle. As the range changes from r_1 to r_2, the amplitude-fading statistics will be a weighted average as

$$p(s) = \int_{m_1}^{m_2} p(m_s) p_S(s|m_s) dm_s, \tag{3}$$

where m_1 and m_2 are the mean signal level at ranges r_1 and r_2, respectively, $p(m_s)$ is the probability function for the mean signal level over the range track, and $p_s(s|m_s)$ is the amplitude-fading distribution given in Eq. (2). The resulting amplitude-fading statistics is not expected to be log-normal unless m is nearly constant.

Figure 5(b) shows the histogram distribution of the symbol amplitude determined from the packets transmitted when the source moves from 5 to 0.5 km. Compared with Fig. 5(a), one finds that the two distributions are similar. One observes that the mean signal energy of the packets fluctuates by ± 3 dB over the track. This small variation (limited range change) is the reason for the qualitatively similar distributions between Figs. 5(a) and 5(b).

III. PHASE ERROR, TRANSITION DETECTOR, AND BER ANALYSIS

A. Symbol phase error

Figure 6(a) shows the differential-phase error between symbols (the error of the differential phase of symbols between data and transmitted signal) determined from the fixed source/receiver data [repeated from Fig. 6(b) of Ref. 10]. As discussed above, the differential phase is determined from the peak of the cross correlation of the matched-filter outputs of two adjacent symbols. The cross correlation of the matched-filter outputs yields $(h_i^* h_{i+1}) S_i^* S_{i+1}$ plus terms containing noise,[10] which will be ignored for the moment, where h_i is the channel impulse response for the ith symbol, denoted by S_i. Assuming that the channel has not changed much within the time period of two symbols, i.e., $h_i^* h_{i+1} \sim I$, one can estimate the differential phase between the two symbols from the cross-correlation result. This is a simple way to estimate the symbol differential phase without requiring a channel equalizer. The differential-phase error [shown in Fig. 6(a)] is obtained by subtracting the true differential phase (between the two symbols) from the measured differential phase. The small differential-phase error (smaller than the phase difference between symbols, i.e., $\pm 90°$) suggests that for the fixed-source data, the symbol phase error can be corrected using a PLL. For practical applications where processing power is limited, it is much simpler to use DPSK signaling without requiring the PLL. For the data shown in Fig. 6(a), there is no bit error since the phase error is $< \pm 90°$.

When either of the source and receiver is moving, one needs to estimate the Doppler shift for each symbol (as discussed above) and apply Doppler correction (including both carrier phase offset and symbol dilatation) to the data. A block diagram for the processing is shown in Fig. 7. For details see Sec. III C. Applying this method to the moving-source data, one can deduce the differential-phase error of symbols as shown in Fig. 6(b). It shows that a high percentage of the symbols are in error for the moving-source data. As explained above, the symbol phase is rapidly changing for a moving source since the phase of each individual path is varying with time. The interference among the time-varying multipath arrivals results in a fast changing differential phase between symbols. To mitigate the fast changing symbol phase, an energy detector that is insensitive to the symbol phase fluctuations is proposed below.

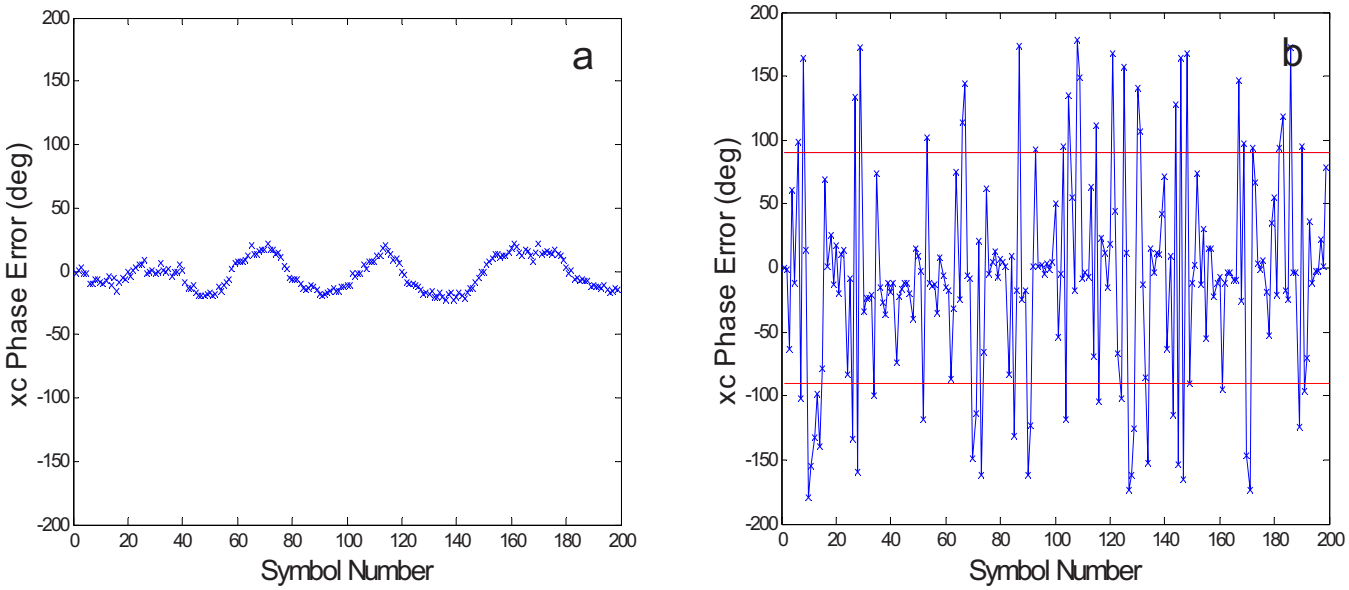

FIG. 6. (Color online) Differential symbol phase error as function of symbol number: fixed-source data (a) and moving-source data (b). Fixed-source data are reproduced from Ref. 10. Moving-source data points (×) are connected by lines to show the magnitude of the phase variation.

B. Transition detectors

In a time-invariant environment without multipaths, one could determine the next symbol from the current symbol using a pair of code sequences proposed previously,[14]

$$T_+ = [C, C] \quad \text{and} \quad T_- = [C, -C], \tag{4}$$

where C is the code sequence expressed as a row vector. The data, after proper synchronization and Doppler correction, are divided into blocks. The data blocks containing two symbols can be expressed as

$$d = [s_n C e^{i\theta_n}, s_{n+1} C e^{i\theta_{n+1}}] + N, \tag{5}$$

where s_n is the nth symbol, $s_n = \pm 1$, θ_n is the random symbol phase, and N denotes the noise; in Eq. (5) the signal amplitude is normalized to 1. The matched-filter output between Eqs. (4) and (5) yields

$$T_+ \cdot d = (s_n e^{i\theta_n} + s_{n+1} e^{i\theta_{n+1}})\rho + \rho_N,$$

$$T_- \cdot d = (s_n e^{i\theta_n} - s_{n+1} e^{i\theta_{n+1}})\rho + \rho_N, \tag{6}$$

where ρ is the autocorrelation function of the code sequence, $\rho = C \cdot C$, and ρ_N denotes the correlation of the code sequence with the noise, $\rho_N = C \cdot N$. Since $\rho > \rho_N$ assuming a high processing gain, the noise contribution is negligible except at very low SNRs. For simplicity we shall drop the noise in the discussions throughout this paper.

In a channel without or with minimal differential-phase error, i.e., $\theta_n = \theta_{n+1}$, one finds $\max|T_+ \cdot d|^2 > \max|T_- \cdot d|^2$, if $s_n s_{n+1} = 1$ (adjacent symbols remain the same, no transition), and $\max|T_- \cdot d|^2 > \max|T_+ \cdot d|^2$, if $s_n s_{n+1} = -1$ (adjacent symbol not the same). Thus by comparing the outputs of the matched filters, Eq. (6), one can determine the next symbol based on the current symbol. However, one finds that this method may not work in a channel that contains a significant differential-phase error since the output squared of the matched filter [Eq. (6)] is a function of the symbol differential phase, which, when in error, can cause incorrect symbol decisions.

To process the moving-source data, which contain a significant differential-phase error, a new pair of transition detector is proposed, which is insensitive to the differential-phase error and therefore robust for symbol estimation/decision. Let C_1 be the first half of the code sequence, and C_2 be the second half of the code sequence, i.e., $C \equiv [C_1, C_2]$. The new transition detectors are given by

$$C_P = [C_2, C_1] \quad \text{and} \quad C_N = [C_2, -C_1]. \tag{7}$$

To see how the new transition detector works, one compares with the (conventional) matched-filter operation. In a multipath time-varying environment, the data of Eq. (5) can be expressed in four half-blocks as

$$d = [s_n h_n C_1, s_n h_{n+1/2} C_2, s_{n+1} h_{n+1} C_1, s_{n+1} h_{n+1+1/2} C_2], \tag{8}$$

where h_n is the impulse response at t_n, and $h_{n+1/2}$ is the impulse response at $t_n + \tau/2$; τ is the symbol duration. The matched filter (using the code sequence C) yields

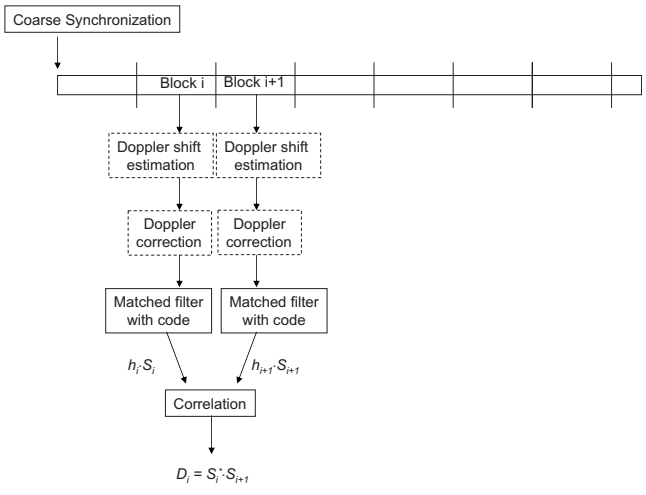

FIG. 7. Block diagram of the cross-correlation method for DPSK signals.

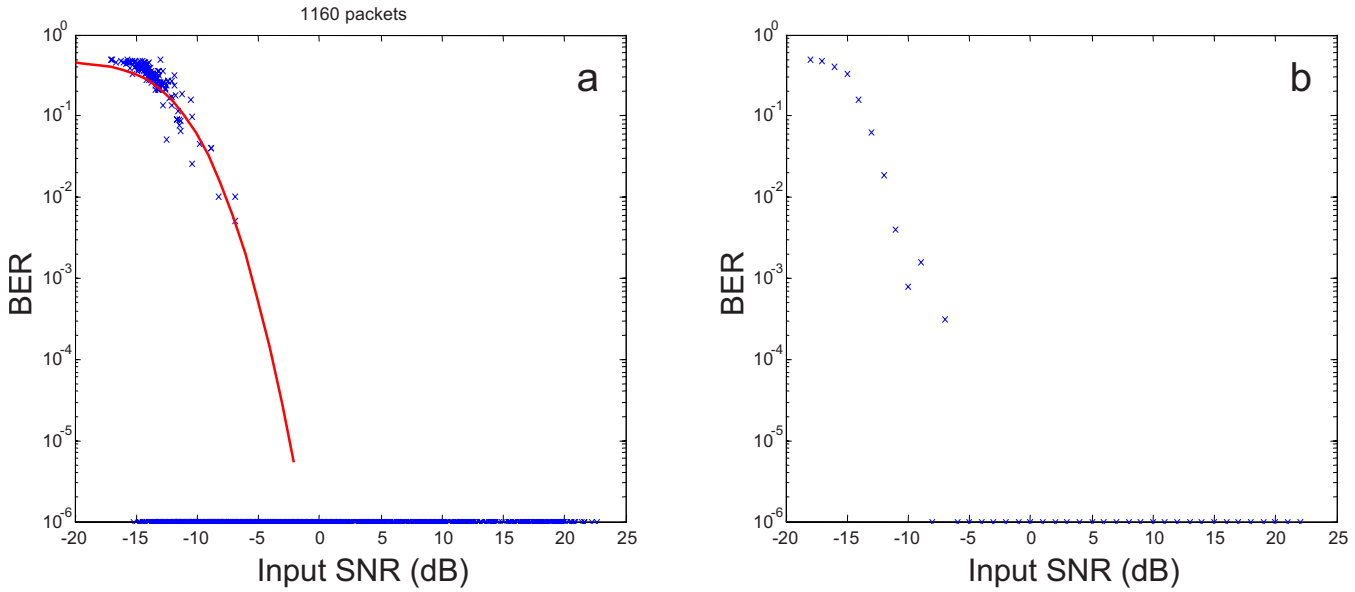

FIG. 8. (Color online) BER (a) and average BER (b) as a function of input SNR using the cross-correlation method for fixed-source data. The solid line is a model prediction. See Ref. 10. Zero BER is represented by 10^{-6} on the logarithmic scale.

$$C \cdot d \simeq [s_n \overline{h}_n \rho, s_{n+1} \overline{h}_{n+1} \rho], \tag{9}$$

where one approximates h_n, $h_{n+1/2}$ by $\overline{h}_n$; the conventional matched filter assumes that the channel is time invariant during a symbol period. The correlation of the matched-filter outputs between the two symbols yields

$$(s_n^* s_{n+1})(\overline{h}_n^* \cdot \overline{h}_{n+1})(\rho \,.\, \rho) = (s_n^* s_{n+1}) |\overline{h}_n^* \overline{h}_{n+1}| e^{i\phi_{n+1}} (\rho \cdot \rho), \tag{10}$$

where ϕ is the differential phase between the symbol due to the random medium, which causes the differential-phase error.

The new transition filter works by the same principle as the (conventional) matched filter, Eq. (9). One finds

$$C_{\pm} \cdot \overline{d} = \overline{h}_{n+1/2} C_{\pm} \cdot [s_n C_2, s_{n+1} C_1], \tag{11}$$

where $\overline{d}$ contains two half-blocks of data, i.e., $\overline{d} = [s_n h_{n+1/2} C_2, s_{n+1} h_{n+1} C_1]$, again assuming that the channel is invariant during one symbol block $\overline{d}$. One can determine whether the next symbol is the same as (or opposite to) the current symbol by comparing the energy of the above transition detector. For example, if $s_{n+1} = s_n$, one has

$$\max |C_{\pm} \cdot \overline{d}|^2 = |s_n \overline{h}_{n+1/2}|^2 (\max |C_{\pm} \cdot C_+|)^2 = |\overline{h}_{n+1/2}|^2 \begin{bmatrix} M^2 \\ \beta^2 \end{bmatrix}, \tag{12}$$

where the autocorrelation function of C_+ is the same as the autocorrelation function of C itself; it has a peak value equal to the length of the code sequence, M, and a sidelobe level equal to 1, and the correlation of C_- against C_+ has a peak value β much less than M; the actual value depends on the sequence used. Thus the C_+ matched filter will yield a higher peak energy than the C_- matched filter. Conversely, if the peak energy of the C_+ matched-filter output is higher than that of the C_- matched filter, it would suggest that $s_{n+1} = s_n$.

Likewise, if $s_{n+1} = -s_n$, one has

$$\max |C_{\pm} \cdot \overline{d}|^2 = |s_n \overline{h}_{n+1/2}|^2 (\max |C_{\pm} \cdot C_-|)^2 = |\overline{h}_{n+1/2}|^2 \begin{bmatrix} \beta^2 \\ M^2 \end{bmatrix}, \tag{13}$$

where the correlation of C_- against itself has a peak value equal to the length of the code sequence and a sidelobe level that varies depending on the sequence; normally close to 1. The correlation of C_+ against C_- has a peak value β much less than M as mentioned above. Since $M \gg \beta$, the C_- matched filter will yield a higher peak energy than the C_+ matched filter. Conversely, if the peak energy of the C_- matched-filter output is higher than that of the C_+ matched filter, it would suggest that $s_{n+1} = -s_n$.

Note that the outputs of Eqs. (12) and (13) are real numbers. The proposed transition $C_{\pm}$ detector is thus not affected by the problem of rapid phase variations and can be applied to the moving-source data. The results will be shown in Secs. III C and III D. The transition detector can also be applied to the fixed-source data. We will first analyze the fixed-source data using the transition detector to compare its performance and with the cross-correlation method of Ref. 10.

The fixed-source data contained 1160 packets with an input SNR varying from −15 to 23 dB. The BER result by cross-correlating the matched-filter outputs of two adjacent symbols is shown in Fig. 8 (Fig. 8 of Ref. 10) assuming DPSK signaling. Figure 8(a) shows the BER as a function of the packet input SNR (the input SNR averaged over each packet) and Fig. 8(b) shows the BER averaged over packets with approximately the same input SNR, plotted as a function of the input SNR. Also shown in Fig. 8(a) is the modeled BER for the DPSK signal. Using the transition filter, the BER result is shown in Fig. 9(a) as a function of the packet input SNR, and the average BER is shown in Fig. 9(b) as a

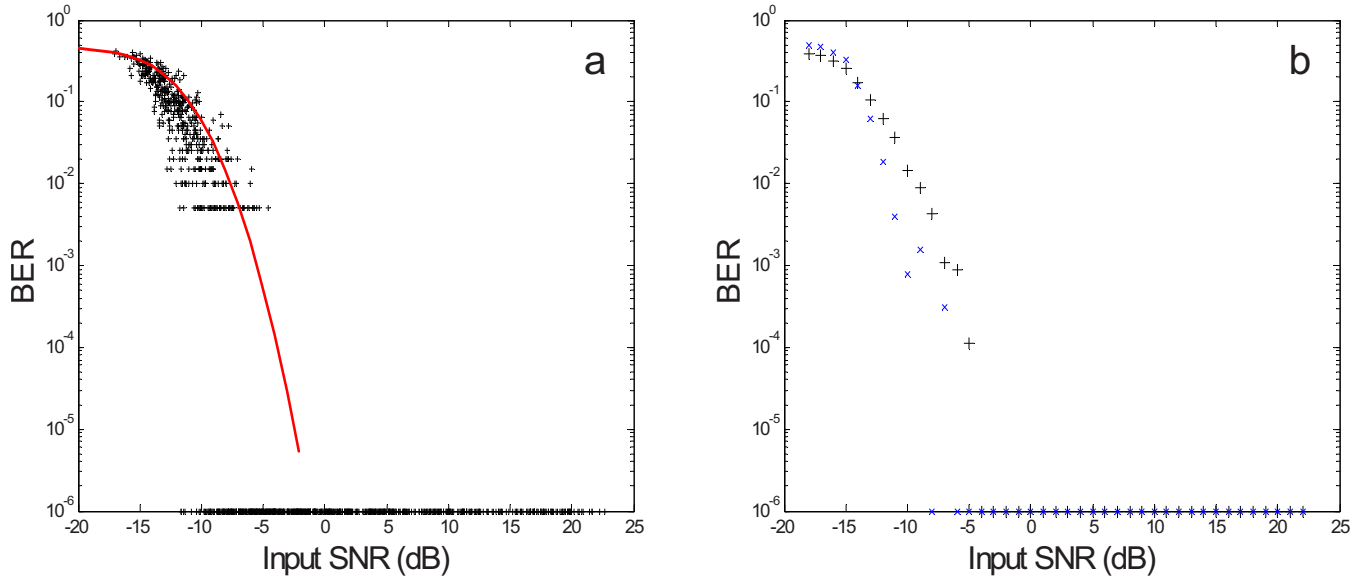

FIG. 9. (Color online) BER (a) and average BER (b) as a function of input SNR using the transition detector method applied to the fixed-source data. × denotes the data of Fig. 8(b) using the cross-correlation method. The solid line is a model prediction. Zero BER is represented by 10^{-6} on the logarithmic scale.

function of the input SNR; both denoted by "+." Also shown in Fig. 9(b) is the average BER repeated from Fig. 8(b), shown by "x." One finds that the BER results using the transition detector are slightly higher than that using the cross correlation of the matched-filter outputs. For the latter method, as pointed out in Ref. 10, the phase estimation can be improved under certain channel conditions by synchronizing the cross-correlation output based on symbols with higher SNRs. The BER in the actual data can be better than expected (modeled) whenever the symbols happen to be properly synchronized. This feature is not available to the transition detector (an energy detector) for LPD applications.

C. Moving-source data results: High SNR

The moving-source data require initial data processing involving Doppler estimation and correction. The block diagram of data processing is shown in Fig. 10. Doppler estimation is done in the base band with two samples with fractional sampling (two samples per chip). After coarse synchronization, the data are divided into overlapping blocks with a length larger than the code length to include the synchronization error. Doppler shift is estimated for each block (symbol) using the wideband ambiguity functions as described above. The signal phase shift (due to Doppler shift) is corrected for each block of data based on the estimated Doppler shift. The data are resampled based on the estimated Doppler shift to correct for time dilation or compression and resynchronized. The symbols are detected by applying the transition filter $C_{\pm}$ to the data to determine if the two adjacent symbols are the same or not. In actual implementations, one finds other ways to simplify the processing. For example, it is simpler to Doppler-shift the transition filter $C_{\pm}$ and apply the filter to the data according to Eqs. (12) and (13).

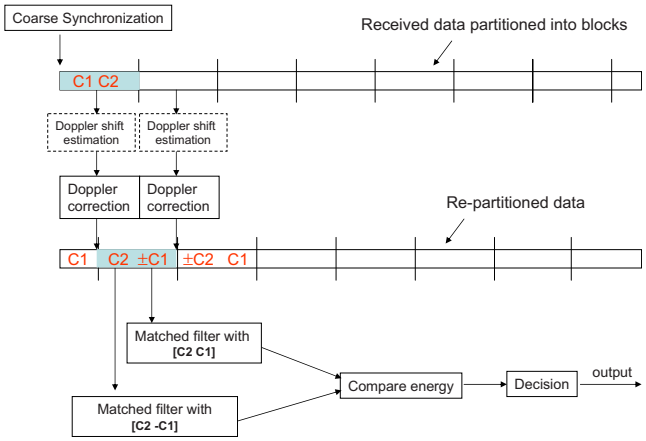

FIG. 10. (Color online) Block diagram of the transition detector method. *C*1 and *C*2 are the first and second halves of the code sequence as described in Sec. III B.

The moving-source data along the track shown in Fig. 1 are processed using the above method, and the result is shown in Fig. 11(b). One finds zero BER except near the end of the run when the source-receiver range is ⩽1 km. The reason is attributed to the fact that at close ranges, the various multipaths arrive with significantly different D/E angles and different Doppler shifts; the spread of the Doppler shifts creates an effective Doppler spread. This finding was supported by Fig. 3(b), which indicates a decreased channel coherence time or a higher Doppler spread at close ranges. To improve the BER at close (⩽1 km) ranges, one needs to estimate the Doppler shift for each path, which is significantly more difficult.

D. BER as a function of decreasing input SNR

To assess the performance of the transition filter at a low input SNR, ambient noise data collected during the same experiment are added to the signal data (see Ref. 10). 2 h of noise data were also collected producing 278 packets of noise. Multiple packets of noise data, randomly chosen, were added to the signal data to generate packets of data with different input SNRs ranging from −13 to +30 dB. The

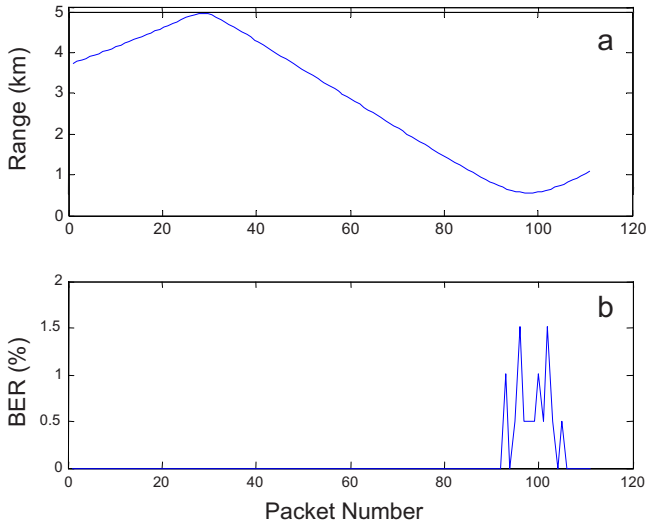

FIG. 11. (Color online) Source-receiver range as a function of time (packet number) repeated from Fig. 3(a) (upper figure). BER as a function of packet number (lower figure).

close range ($\leqslant$1 km) data are excluded from this analysis as remarked above. BER is then deduced as a function of input SNR. The result is shown in Fig. 12(a) as a function of the packet input SNR. The average BER is shown in Fig. 12(b) as a function of input SNR. Compared with the average BER determined from the fixed-source data [repeated from Fig. 9(b), shown by +], one finds a performance degradation of 1–2 dB. Note that while the cross-correlation method failed for the moving-source data, the transition filter method works pretty well for both fixed- and moving-source data.

IV. PROBABILITY OF DETECTION AND COUNTERDETECTION RANGE

The probability of detection (P_D) depends on the construction of the detector; the more the detector knows about the signal, the more features the detector can use to improve the detection. If the signal waveform is known, one can employ a coherent detector, e.g., a matched filter, which often yields a high P_D given the processing gain derivable from the signal. Noiselike signals are difficult to detect using a coherent detector as the signal is random and difficult to replicate compared with, for example, an impulselike signal. This also favors the DSSS signaling as compared with, for example, frequency-hopping frequency-shift-keying signaling. For the latter, while the average SNR is low, the SNR for information carrying frequency bins is high. As a result, the repeated (or time-varying) frequency hopping pattern may alert the operator to the presence of a man-made signal. Once the operator is alerted, more sophisticated signal processing can be used to search for the signal parameters and construct an improved detector.

If the signal waveform is not known, one is left with an energy detector. A commonly used energy detector is the spectrogram, which detects a sudden increase in the SNR as a function of frequency and time. This normally requires a fairly good SNR (say 5 dB) over the signal frequency band and is most effectively done by a human being who can interactively adjust the Fourier transform window to match the signal. A computer-aided detector needs to know the signal bandwidth and signal duration, as mismatch in bandwidth and duration between the signal and detector can significantly decrease the detection performance. The mismatch in bandwidth is self-evident, as incorrect bandwidth results in a loss of part of the signal energy and addition of more noise energy. Likewise, the signal duration also influences the detector performance (see Sec. IV C). If the integration time is much longer than the signal duration, it effectively reduces the SNR as more noise is included in the detector output. Without knowing the signal duration, a narrowband detector is often used to detect narrowband energy and a broadband pulse detector (i.e., short integration time) is commonly used to detector a burst energy. The detectors will alert the opera-

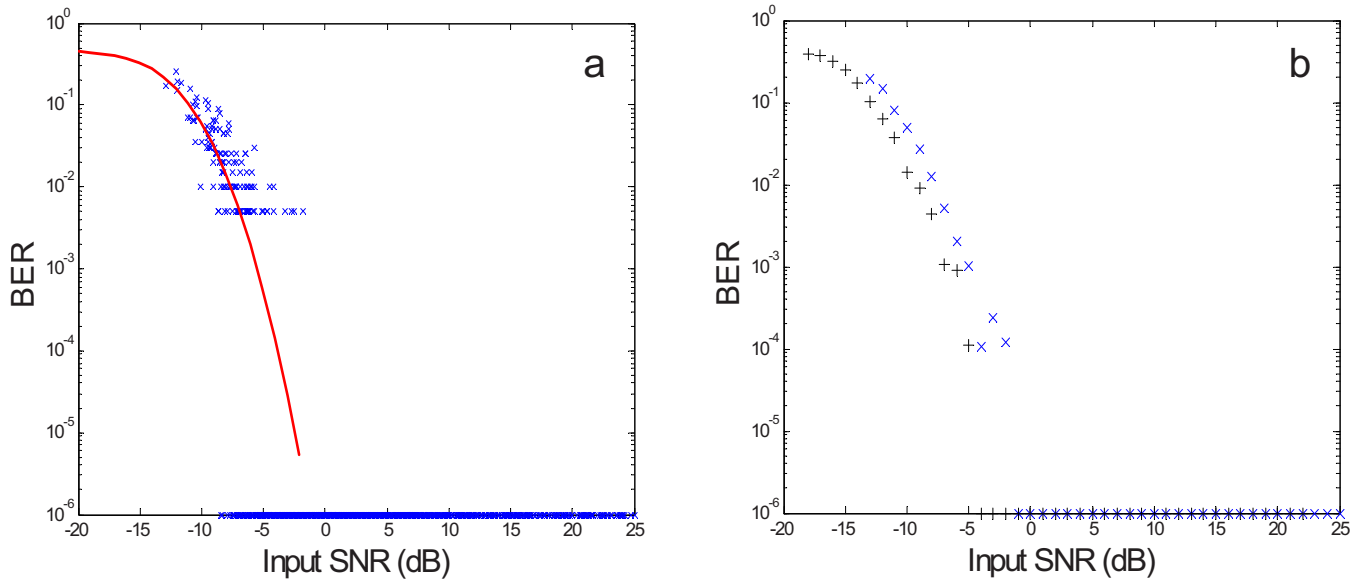

FIG. 12. (Color online) BER (a) and average BER (b) as a function of input SNR using the transition detector method applied to the moving-source data. + denotes the fixed-source data of Fig. 9(b). The solid line is a model prediction shown in Fig. 8(a). Zero BER is represented by 10^{-6} on the logarithmic scale.

tor for a potential signal of interest, when P_D exceeds the recognition differential for the signal of interest.

The P_D for an energy detector depends very much on the input SNR. Pseudorandom noiselike DSSS signals with an input level lower than the ambient noise (e.g., SNR ~ -8 dB within the signal band) are difficult to detect by a narrowband or broadband energy detector assuming an unalerted listener. As input SNR increases (as when source-receiver ranges decrease), the probability that the signal will be detected increases. From a system point of view, the question is as follows: At what range will the signal be detected or what is the counterdetection range? The answer is channel dependent. It requires a determination of the P_D and the probability of false alarm (P_{FA}) as a function of input SNR, for a given signal-fading distribution. This topic is addressed in Sec. IV A. To determine the input SNR, one needs to calculate the signal transmission loss (TL) as a function of source-receiver range for a given source power and noise level. This calculation is done for a typical shallow water environment in Sec. IV B. This section also shows the P_D as a function of source-receiver range for a given P_{FA}. The analysis involves two receivers. One is the intended (friendly) receiver and the other is the unfriendly receiver, the interceptor. The objective is to minimize P_D of the signal by the interceptor for a given P_{FA}, which means the lower the SL, the better the result. On the other hand, the SL of the transmitting node should be high enough so that the message is received at the intended receiver with a high enough SNR for decoding the message. The SL is a system parameter that needs to be determined first. See Sec. IV B.

A. P_D and P_{FA} of an energy detector

The P_D and P_{FA} for a broadband pulse energy detector are well known for a nonfading channel[15,16] and a Rayleigh-fading channel,[1] but not for a log-normal-fading channel. The data as discussed above indicate that the fading statistics for the DSSS signal in an underwater acoustic channel follows the log-normal distribution.[10] A derivation of the P_D and the P_{FA} is reviewed below, which can be generalized to include the log-normal distribution.

1. Nonfading channel

For a nonfading channel, the signal (each symbol) has a constant amplitude a. Assuming additive white Gaussian noise, with a Rayleigh amplitude distribution, the probability of detection is given by the following two statistics:

$$p_r(x) = \begin{cases} \dfrac{x}{\sigma_N^2} \exp(-(x^2+a^2)/2\sigma_N^2) I_0(ax/\sigma_N^2) & \text{with signal present} \\ \dfrac{x}{\sigma_N^2} \exp(-x^2/2\sigma_N^2) & \text{with signal absent,} \end{cases} \tag{14}$$

where σ_N is the noise variance and I_0 is the modified Bessel function of zeroth order. Let $Y=X^2$ be the square-law output of an energy detector. It can be shown that the probability density function of Y becomes

$$p_r(y) = \begin{cases} \dfrac{1}{2\sigma_N^2} \exp(-(y/2\sigma_N^2+\gamma)) I_0(2\sqrt{\gamma y/2\sigma_N^2}) & \text{with signal present} \\ \dfrac{1}{2\sigma_N^2} \exp(-y/2\sigma_N^2) & \text{with signal absent,} \end{cases} \tag{15}$$

where $\gamma = a^2/2\sigma_N^2$ is the mean SNR at the input of an energy detector (mean input SNR). Given a threshold η, let the P_{FA} be the probability that the noise energy is higher than η. Using the lower equation of Eq. (15), one has

$$P_{\mathrm{FA}} = \int_{\eta}^{\infty} \frac{1}{2\sigma_N^2} \exp\left[-\frac{y}{2\sigma_N^2}\right] dy = \exp\left[-\frac{\eta}{2\sigma_N^2}\right]. \tag{16}$$

The probability of detection, P_D, is the probability that the signal plus noise energy is higher than η. Using the upper equation of Eq. (15), it can be expressed as a function of the P_{FA} as follows:

$$P_D = \int_{\eta}^{\infty} \frac{1}{2\sigma_N^2} \exp(-(y/2\sigma_N^2+\gamma)) I_0(2\sqrt{\gamma y/2\sigma_N^2}) dy$$
$$= \int_{-\ln(P_{\mathrm{FA}})}^{\infty} \exp(-(u+\gamma)) I_0(2\sqrt{\gamma u}) du, \tag{17}$$

where $u = y/2\sigma_N^2$ is the integration variable and γ is the mean input SNR.

2. Fading channel

The P_{FA} in a fading channel is the same as that in a nonfading channel [Eq. (16)] for a given threshold η. The P_D can be expressed as

$$P_D = \int_0^\infty p_{D|S} p_S(s) ds$$
$$= \int_0^\infty p_S(s) \int_\eta^\infty \frac{1}{2\sigma_N^2} \exp[-(y+s^2)/2\sigma_N^2] I_0(s\sqrt{y}/\sigma_N^2) dy ds$$
$$= \int_\eta^\infty \frac{1}{2\sigma_N^2} \exp(-y/2\sigma_N^2) A(y) dy, \quad (18)$$

where $P_{D|S}$ is the conditional probability of detection for a signal with an instantaneous signal amplitude s as given in Eq. (17), p_s is the amplitude distribution of the signal, and

$$A(y) = \int_0^\infty \exp(-s^2/2\sigma_N^2) I_0(s\sqrt{y}/\sigma_N^2) p_s(s) ds. \quad (19)$$

For a Rayleigh-fading channel,

$$p_S(s) = \begin{cases} \frac{s}{\sigma_s^2} \exp\left(-\frac{s^2}{2\sigma_s^2}\right) & \text{if } s > 0 \\ 0 \quad \text{if } s \leqslant 0. \end{cases} \quad (20)$$

One finds

$$A(y) = \int_0^\infty \exp(-s^2/2\sigma_N^2) I_0(s\sqrt{y}/\sigma_N^2) \frac{s}{\sigma_s^2} \exp(-s^2/2\sigma_s^2) ds$$
$$= \frac{\sigma_N^2}{\sigma_s^2 + \sigma_N^2} \exp\left[\frac{\sigma_s^2 y}{2\sigma_N^2(\sigma_s^2+\sigma_N^2)}\right] \quad (21)$$

and

$$P_D = \int_\eta^\infty \frac{1}{2\sigma_N^2} \exp(-y/2\sigma_N^2) \frac{\sigma_N^2}{\sigma_s^2+\sigma_N^2} \times \exp\left[\frac{\sigma_s^2 y}{2\sigma_N^2(\sigma_s^2+\sigma_N^2)}\right] dy$$
$$= \exp\left[\frac{-\eta}{2(\sigma_s^2+\sigma_N^2)}\right], \quad (22)$$

where η is the threshold set by P_{FA}. The relationship between P_D and P_{FA} can be expressed as follows:

$$P_{\mathrm{FA}} = (P_D)^{1+\gamma}, \quad (23)$$

where $\gamma = 2\sigma_s^2/2\sigma_N^2 = \sigma_s^2/\sigma_N^2$ is the mean input SNR.

For a log-normal-fading channel, the amplitude-fading statistics are given by Eq. (2) for the signal present case. Substituting the log-normal distribution into the $A(y)$, Eq. (19), one finds

$$P_D = \int_\eta^\infty \frac{1}{2\sigma_N^2} \exp(-y/2\sigma_N^2) A(y) dy$$
$$= \int_\eta^\infty \frac{1}{2\sigma_N^2} \exp(-y/2\sigma_N^2) \int_0^\infty \exp(-s^2/2\sigma_N^2) \times I_0(s\sqrt{y}/\sigma_N^2) \frac{1}{\sqrt{2\pi}\sigma_s} s^{-1} \exp\left(-\frac{(\ln s - \mu_s)^2}{2\sigma_s^2}\right) ds dy. \quad (24)$$

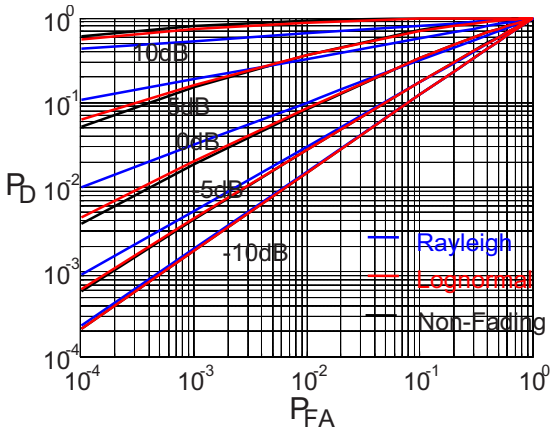

FIG. 13. (Color online) Receiver operation characteristic curves showing P_D as a function of P_{FA} for various SNRs and signal-fading distributions.

The relationship between the detection probability and the false alarm probability is

$$P_D = \int_{-\ln(P_{\mathrm{FA}})}^\infty e^{-u} \int_0^\infty e^{-\gamma\alpha^2 s^2} I_0(2s\alpha\sqrt{\gamma u}) \frac{1}{\sqrt{2\pi}\sigma_s} s^{-1} \times \exp\left(-\frac{(\ln s - \mu_s)^2}{2\sigma_s^2}\right) ds du, \quad (25)$$

where $\gamma = E(S^2)/2\sigma_N^2 = e^{2\mu_s + 2\sigma_s^2}/2\sigma_N^2 = \xi^{-2}/2\sigma_N^2$ is the mean input SNR and $\xi = e^{-\mu_s - \sigma_s^2}$.

Using Eqs. (17), (23), and (25), one can calculate P_D as a function of P_{FA} for a given input SNR, the so called receiver operation characteristic (ROC) curve, for nonfading, Rayleigh-fading, and log-normal-fading cases. The results are shown in Fig. 13. For the log-normal fading, we have used $\mu_s = -1.6449$ and $\sigma_s^2 = 0.0304$ obtained from the distribution of input signal amplitude.

The ROC curve (Fig. 13) is commonly used for detection analysis. It shows the dependence of P_D as a function of P_{FA} for a given SNR. The same results can also be displayed in a different manner, for example, showing the P_D as a function of SNR for a given P_{FA} as will be done in the next section to calculate the counterdetection. One notes from Fig. 13 that the P_D versus P_{FA} relation based on the log-normal statistics is much closer to the nonfading case than to the Rayleigh-fading case. There are differences between the log-normal- and nonfading cases, which are not clearly seen in a log-log plot.

B. Counterdetection range

As P_D is a function of the (mean) input SNR and the input SNR is a function of source-receiver range for a given SL, one can calculate the P_D as a function of source-receiver range for a given P_{FA}. Counterdetection range will be defined as the range below which $P_D > 0.5$. To model the SNR at the receiver, we calculate the TL in the TREX04 environment using the range-dependent acoustic model parabolic equation (RAM PE) model.[17] The result is shown in Fig. 14 for a 17 kHz signal. Superimposed is a sonar-equation-based calculation, which assumes spherical spreading to a range of

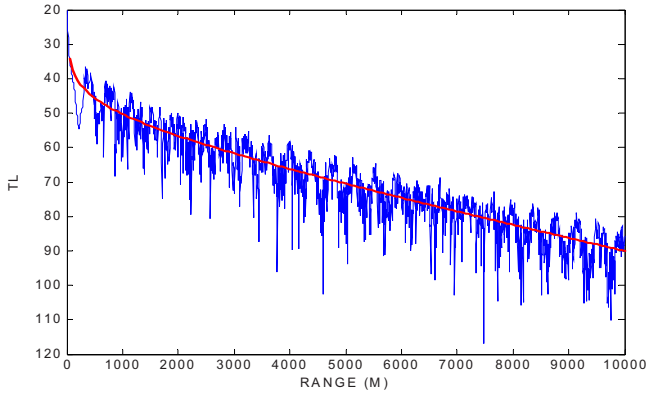

FIG. 14. (Color online) TL as a function of range using the RAM PE model. The smooth line is the empirical model calculation based on sound attenuation by sea water.

50 m and cylindrical spreading beyond 50 m. For absorption by the water medium we use the following expression due to Thorp:[18]

$$\alpha = \left(\frac{0.1f^2}{1+f^2} + \frac{40f^2}{4100+f^2} + 2.75 \times 10^{-4} f^2 + 0.003 \right) \times 0.875, \tag{26}$$

where α is the absorption loss in dB/km, f is the acoustic frequency in kHz, and 0.875 is a depth correction factor determined by fitting the RAM calculation; the original formula is for a depth of 1000 m. To determine the SNR at the receiver, we note that at 17 kHz, the noise is dominated by wind generated noise, with a spectral level given by[19]

$$10 \log N(f) = 50 + 7.5w^{1/2} + 20 \log f - 40 \log(f + 0.4), \tag{27}$$

where w is the wind speed in m/s. Assuming $w = 10$ m/s, one finds NL = 49 dB. Given the TL and noise level, one can calculate the SNR as a function of range for a given SL. Given the SNR one can then calculate the P_D as a function of range for a given P_{FA} using the equation in Sec. IV A. The following are the numerical results shown in Fig. 15 for P_D as a function of range assuming three SLs: 143, 155, and 164 dB and $P_{\mathrm{FA}} = 0.01$. These SLs are needed for communications to an intended (friendly) receiver at a range of ~2, 4, and 7 km. Based on Fig. 12(b), a minimum input SNR of −10 dB is required at the intended receivers to achieve a minimum (<1%) BER. The minimum input SNR is used with TL to determine the minimum SLs.

Figures 15(a) and 15(b) show the P_D as a function of the source-to-interceptor range for Rayleigh signal-fading and log-normal signal-fading statistics, respectively. One finds that the counterdetection range (for $P_D \geqslant 0.5$) is approximately 1.3, 3.6, and 5.8 km for the three SLs assuming Rayleigh-fading statistics and approximately 1.4, 3.8, and 6.1 km for the three SLs assuming log-normal-fading statistics. Naturally, the higher the SL, the greater the counterdetection range. As expected, the counterdetection range for an energy detector is shorter than the communication range to a friendly receiver using a matched filter. Hence, the communication signal will not likely be detected by an interceptor located outside the communication range (or the operation area). But as the interceptor approaches one of the transmitting nodes, detection by the interceptor is unavoidable. The hope is that the interceptor remains unalerted, such as when the signal is noiselike.

Note that at $P_D = 0.5$ the differences in the counterdetection ranges are relatively small between the two signal-fading scenarios. However, if the detection ranges were defined at a higher P_D, e.g., $P_D = 0.9$, the differences between the two cases would be significant. The difference is that the P_D increases faster with a decreasing range for the log-normal than for the Rayleigh distribution.

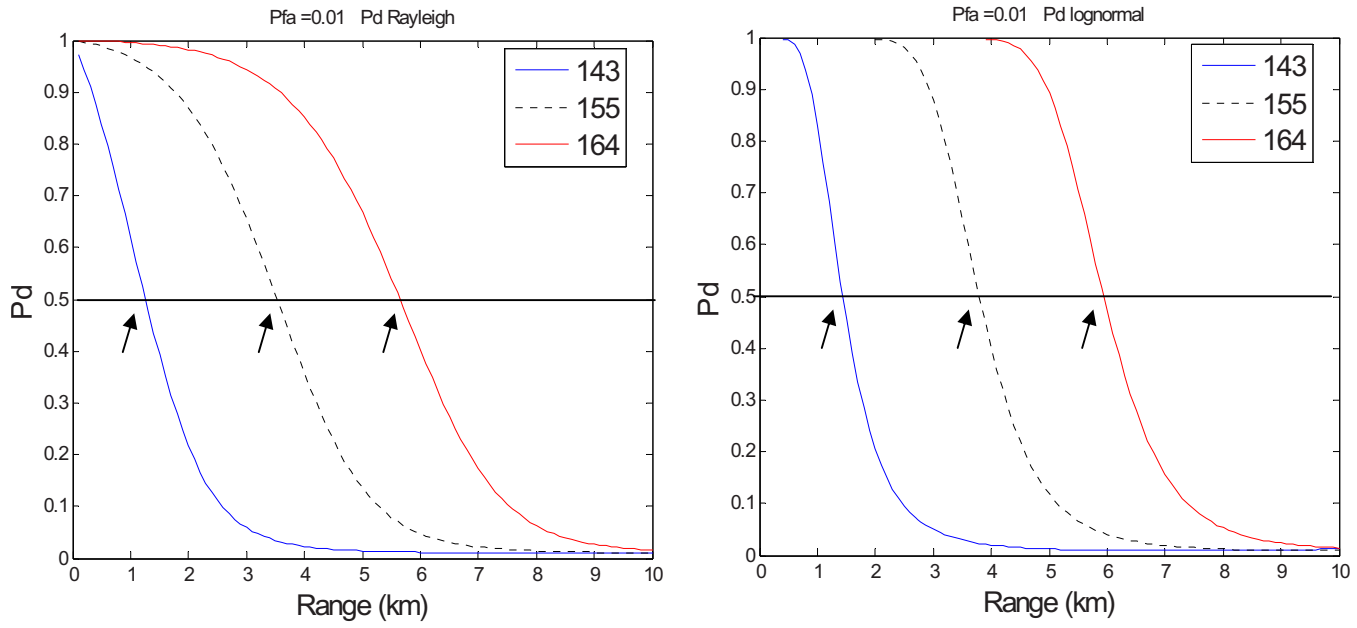

FIG. 15. (Color online) P_D as a function of source-receiver range for $P_{\mathrm{FA}} = 0.01$ for three assumed SLs. The left figure assumes Rayleigh signal fading and the right figure assumes log-normal signal fading.

C. Integrating over multiple observations

If the signal is present for a long period of time, the interceptor, if alerted, can improve its detection by integrating the signal energy over multiple observations (normally in postprocessing after the operator has been alerted.) Let T be the sample interval and $y(t)$ be the *energy* at time t. Assuming that all samples are independent, then the integrated energy over a dwell time τ_d can be approximated as follows:

$$z = \frac{1}{T}\int_0^{\tau_d} y(t)dt \approx \sum_{k=0}^{N_s-1} y(kT), \tag{28}$$

where $N_s = \tau_d / T$ is the number of samples.

For large N_s, Z is approximately Gaussian distributed. In contrast with Eq. (16), the P_{FA} for a given threshold η_z is given by

$$P_{\mathrm{FA}} = \int_{\eta_z}^{\infty} \frac{1}{\sqrt{2\pi}\sigma_2} \exp\left[-\frac{(z_z-\mu_2)^2}{2\sigma_2^2}\right] dz \equiv Q\left(\frac{\eta_z-\mu_2}{\sigma_2}\right)$$

$$= Q\left(\frac{\eta_z - 2_s\sigma_N^2}{2\sigma_N^2\sqrt{N_s}}\right), \tag{29}$$

where $\mu_2 = 2N_s\sigma_N^2$ and $\sigma_2^2 = 4N_s\sigma_N^4$ are the mean and variance of the noise only case.

Assuming that the signal, y, follows a log-normal distribution (Sec. IV A), then the probability distribution function of z is given by (details given in the Appendix)

$$P(z) = \frac{1}{\sqrt{2\pi}\sigma_1} \exp\left[-\frac{(z-\mu_z)^2}{2\sigma_z^2}\right], \tag{30}$$

where

$$\mu_z = 2N_s\sigma_N^2(1+\gamma),$$

$$\sigma_z^2 = 4N_s\sigma_N^4(1+2\gamma) + N_s\exp(4\mu_s + 4\sigma_s^2)[\exp(4\sigma_s^2) - 1], \tag{31}$$

where $\gamma = E_s(s^2)/2\sigma_N^2 = \exp(2\mu_s + 2\sigma_s^2)/2\sigma_N^2$ is the mean input SNR, and μ_s and σ_s^2 are the parameters of the log-normal distribution [Eq. (2)]. In contrast with Eq. (25), the P_D is now given by [see Eq. (A11)]

$$P_D = Q\left(\frac{\eta_z - 2N_s\sigma_N^2(1+\gamma)}{\sqrt{4N_s\sigma_N^4[1+2\gamma+\gamma^2(\exp(4\sigma_s^2)-1)]}}\right). \tag{32}$$

Using Eqs. (29) and (32), one plots the P_D as a function of input SNR for a $P_{\mathrm{FA}} = 0.01$ as shown in Fig. 16 for various values of N_s. Comparing $N_s = 25$ with $N_s = 1$, one finds ~10 dB improvement in SNR at $P_D = 0.5$. Thus, knowing that the signal bandwidth and hence T and that the signal is at least $N_s T$ long, the signal could be detected by long integration time. As an example, an input SNR of −8 dB, which has a low probability being detected by a broadband pulse detector, could now be detected because the integration yields an effective +2 dB SNR. This assumes that the operator has been alerted that there is a man-made signal and turns on the search for the signal parameters and long integration detector.

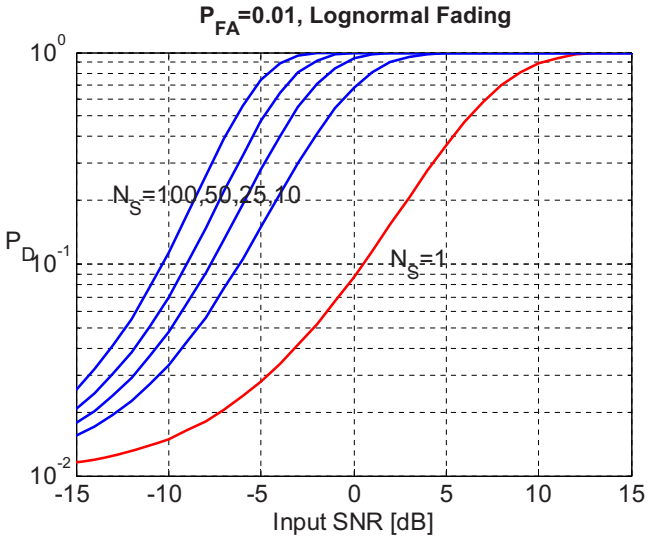

FIG. 16. (Color online) P_D as a function of input SNR for $P_{\mathrm{FA}} = 0.01$ for different values of N_s.

Figure 17 shows the probability density distributions of the noise only (upper figure) and signal plus noise (lower figure) for the $N_s = 1$ and $N_s = 25$ cases. For the $N_s = 1$ case, $z = y$, one finds that the noise density distribution decreases exponentially with energy. With the signal present, while the signal (amplitude) has a log-normal distribution, the probability density distribution of the signal plus noise decreases with the signal+noise energy. For $N_s = 25$, the probability density is approximately normally distributed. While y and z/N_s have the same mean and same SNR in Fig. 17, they have different probability distributions. The fact that z has the same probability distribution for the signal-plus-noise and noise only cases is the reason that P_D for $N_s = 25$ is large for $P_{\mathrm{FA}} = 0.01$ (higher than that for $N_s = 1$, for the same P_{FA}). One may argue that a smaller P_{FA} (e.g., $P_{\mathrm{FA}} = 0.01/25$ or 4×10^{-4}) should be used for the $N_s = 25$ case, since there are

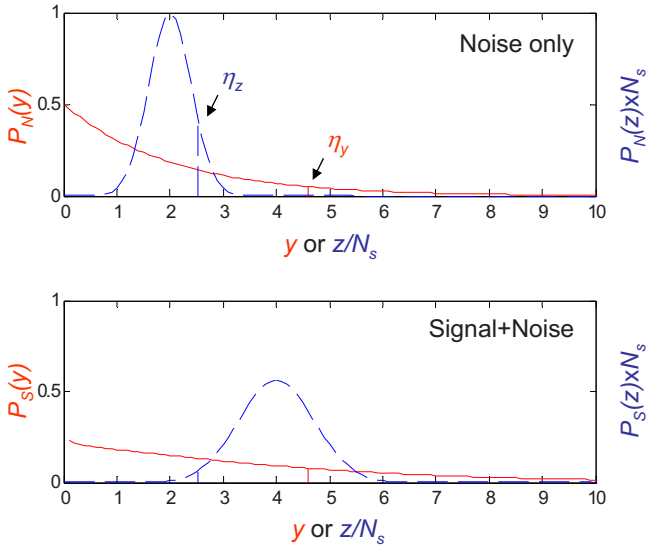

FIG. 17. (Color online) Probability distribution of noise only (upper figure) and signal plus noise (lower figure). The solid line is for $N_s = 1$, showing the probability as a function of y. The dashed line is for $N_s = 25$, showing the probability $p(z) \times N_s$ as a function of z/N_s.

more counts of false alarms for $N_s=25$ than for $N_s=1$. Note that for the $N_s=25$ case, the detector does not require the signal to be detectable for each sample interval T but only for the entire time period of $25T$. What values of P_{FA} to use are system dependent and likely also environment dependent; it is beyond the scope of this paper. This section presents only an example. One can calculate P_D versus P_{FA} based on the equations in the Appendix.

V. SUMMARY AND DISCUSSION

The rapid symbol phase change as a function of time for PSK signals has been well noted in underwater acoustic communications. For DSSS signaling, each symbol covers many chips and the symbol phase change, accumulating over the chips, can be large. The symbol phase change can be caused by a random medium, which produces different phases for different multipath arrivals. The TREX04 data showed that the differential phase between adjacent symbols for fixed-source and fixed-receiver transmissions was smaller than $\pm 90°$, suggesting that the phase imposed by the random medium changes gradually between symbols.[10] In that case, DPSK signals can be decoded by cross-correlating the matched-filter outputs of two adjacent symbols. For a moving source or receiver, the fact that the range is changing with time also contributes to the symbol phase change. The additional phase change contains both a deterministic as well as a random component; the latter is a result of multipaths traveling through different parts of the random medium at different times. The TREX04 data showed that the differential phase between adjacent symbols for a moving-source and a fixed-receiver transmission is often larger than $\pm 90°$. In this case, the cross-correlation method does not work for the moving-source data.

A pair of transition detectors, based on the same principle as the matched filter, are proposed in this paper for moving, as well as for fixed source data. Whether adjacent symbols are of the same kind or opposite kind is determined by the energy of the transition detectors. The transient (pulse) detector, being an energy detector, is insensitive to the symbol phase fluctuations. The method is applied to the TREX04 data. At-sea noise was added to the signal data to generate data of low input SNR. BER was measured for an input SNR from +25 to −15 dB. The moving-source data yielded a comparable, slightly degraded BER compared with the fixed-source data using the same method. For the fixed-source data, the performance is slightly degraded compared with that using the cross-correlation method. Whether the performance degradation is data dependent remains to be investigated.

The purpose of low SNR DSSS communications is to minimize the probability of detection and interception by a hostile interceptor. Since the probability of detection and interception is detector specific, assuming that the detector does not have infinite resources to employ different kinds of detectors simultaneously, the first line of defense is to minimize the probability of detection by the two most popular detectors, i.e., a narrowband energy detector and a broadband pulse detector, under the assumption that the detector has no a priori knowledge of the signal parameters or the signal parameters are constantly changing with time. Obviously, one does not have to worry about narrowband energy detector for DSSS communications. Anticipating the use of a broadband pulse detector, the question is at what range will the signal be detected, the counterdetection range. The answer is case dependent. As an illustration, we assume a typical shallow water environment and analyze the probability of detection as a function of range. Three SLs are used for three intended (friendly) receivers. Counterdetection range is calculated based on $P_D>0.5$ and $P_{\mathrm{FA}}=0.01$. The analysis assumes a single receiver, and can be extended to an array of receivers using the directivity index. As expected, the lower the SL, the shorter the counterdetection range.

If the interceptor is aware of a man-made signal in the water, and that it has many snapshots of data to investigate, the interceptor could improve its detection probability by integrating the signal energy over the snapshots of data. The probability of detection using a long integration time is also analyzed in this paper.

Generally, one expects the lower the input SNR, the lower the probability of detection, as illustrated by the numerical examples given above. But communications at a lower input SNR comes with the price of a lower data rate for DSSS signaling. It requires a longer transmission time to get the same throughput compared with a higher data rate, higher SNR communications scheme. One expects that all signals could eventually be detected if the detector knows about the existence of the signal and has infinite resources to investigate the signal properties. By way of illustration, it is pointed out that low SNR DSSS signal could be detected by long integration even using an incoherent detector, if such signals are known to be present. In practice, one does not have infinite resources. The advantage of low SNR DSSS communications is, from the practical point of view, that it has a low input SNR and it is noiselike. It has a LPD by a broadband pulse energy detector. In doing so, as long as the operator remains unalerted of the existence of the signal, the signaling can be considered covert.

ACKNOWLEDGMENT

This work is supported by the Office of Naval Research. We are grateful to the NRL Acoustic Division personnel who supported and conducted the TREX04 experiment.

APPENDIX: PROBABILITY OF DETECTION AND PROBABILITY OF FALSE ALARM WITH MULTIPLE OBSERVATIONS

Let T be the sample interval and $y(t)$ be the energy at time t. Assuming that all samples are independent, then the integrated energy over a dwell time τ_d can be approximated as follows:

$$z=\frac{1}{T}\int_0^{\tau_d} y(t)dt \approx \sum_{k=0}^{N_s-1} y(kT), \tag{A1}$$

where $N_s=\tau_d/T$ is the number of samples. For large N_s, Z may be approximately Gaussian distributed.

Assuming Gaussian distribution for z, one has

$$P_D = \int_{\eta_z}^{\infty} \frac{1}{\sqrt{2\pi}\sigma_1} \exp\left[-\frac{(z-\mu_1)^2}{2\sigma_1^2} \right] dz \equiv Q\left(\frac{\eta_z - \mu_1}{\sigma_1} \right), \tag{A2}$$

where Q is defined in Eq. (29). Thus to calculate P_D, one needs only to evaluate the mean and variance of the signal plus noise.

With the signal present, the mean and the variance of $y_k = y(kT)$ for a given instantaneous signal energy s in the presence of AWGN are given by

$$\mu_a = 2\sigma_N^2 + s^2 \quad \text{and} \quad \sigma_a^2 = 4\sigma_N^2(\sigma_N^2 + s^2). \tag{A3}$$

Letting the distribution of Y_k for a given s be $p_{y_k|s}(y_k|s)$, the distribution of Y_k becomes

$$p_{\gamma_k}(y_k) = \int p_{\gamma_k|S}(y_k|s) p_s(s) ds. \tag{A4}$$

Thus, the mean and the variance of Y_k are obtained as follows:

$$\begin{aligned} \mu_k &= \int y_k p_{\gamma_k}(y_k) dy_k = \int \int y_k p_{\gamma_k|S}(y_k|s) p_S(s) ds dy_k \\ &= \int \int y_k p_{\gamma_k|S}(y_k|s) dy_k \cdot p_S(s) ds \\ &= \int (2\sigma_N^2 + s^2) p_S(s) ds = 2\sigma_N^2 + E_s(s^2) = 2\sigma_N^2(1+\gamma) \end{aligned} \tag{A5}$$

and

$$\begin{aligned} \sigma_k^2 &= E(y_k^2) - [E(y_k)]^2 = \int y_k^2 p_{\gamma_k}(y_k) dy_k - \mu_k^2 \\ &= \int \int y_k^2 p_{\gamma_s|s}(y_k|s) p_S(s) ds dy_k - \mu_k^2 \\ &= \int (\sigma_a^2 + \mu_a^2) p_s(s) ds - \mu_k^2 \\ &= \int (8\sigma_N^4 + 8\sigma_N^2 s^2 + s^4) p_s(s) ds - \mu_k^2 \\ &= 8\sigma_N^4 + 8\sigma_N^2 E_s(s^2) + E_s(s^4) - \mu_k^2 \\ &= 4\sigma_N^4(1+2\gamma) + E_s(s^4) - [E_s(s^2)]^2 \\ &= 4\sigma_N^4(1+2\gamma) + \mathrm{var}(s^2) \end{aligned} \tag{A6}$$

where $E_s(s^2)$ and $\mathrm{var}(s^2)$ are the mean and variance of the signal intensity, and $\gamma = E_s(s^2)/2\sigma_N^2$ is the mean input SNR. For large N_s, assuming a Gaussian distribution for z, the mean and variance of z are as follows:

$$\mu_1 = 2N_s\sigma_N^2(1+\gamma), \quad \sigma_1^2 = 4N_s\sigma_N^4(1+2\gamma) + N_s\,\mathrm{var}(s^2). \tag{A7}$$

The corresponding detection probability is

$$\begin{aligned} P_D &= \int_{\eta}^{\infty} \frac{1}{\sqrt{2\pi}\sigma_1} \exp\left[-\frac{(z-\mu_1)^2}{2\sigma_1^2} \right] dz = Q\left(\frac{\eta - \mu_1}{\sigma_1} \right) \\ &= Q\left(\frac{\eta - 2N_s\sigma_N^2(1+\gamma)}{\sqrt{4N_s\sigma_N^4(1+2\gamma) + N_s\,\mathrm{var}(s^2)}} \right). \end{aligned} \tag{A8}$$

For a Rayleigh-fading channel, using Eq. (20), one finds $\mathrm{var}(s^2) = 4\sigma_s^4$ and

$$P_D = Q\left(\frac{\eta - 2N_s\sigma_N^2(1+\gamma)}{\sqrt{4N_s\sigma_N^4(1+2\gamma) + 4N_s\sigma_s^4}} \right), \tag{A9}$$

where $\gamma = E_s(s^2)/2\sigma_N^2 = \sigma_s^2/\sigma_N^2$ is the mean input SNR. The relationship between the detection probability and the false alarm probability is given by

$$P_D = Q\left(\frac{Q^{-1}(P_{\mathrm{FA}}) - \gamma\sqrt{N_s}}{\sqrt{1+2\gamma+4\sigma_s^4/4\sigma_N^4}} \right) = Q\left(\frac{Q^{-1}(P_{\mathrm{FA}}) - \gamma\sqrt{N_s}}{1+\gamma} \right). \tag{A10}$$

For a log-normal-fading channel, using Eq. (2), one finds $E_s(s^2) = \exp(2\mu_s + 2\sigma_s^2)$ and $\mathrm{var}(s^2) = \exp(4\mu_s + 4\sigma_s^2) \times [\exp(4\sigma_s^2) - 1]$. Equation. (A8) then yields

$$P_D = Q\left(\frac{\eta - 2N_s\sigma_N^2(1+\gamma)}{\sqrt{4N_s\sigma_N^4[1+2\gamma+\gamma^2(\exp(4\sigma_s^2)-1)]}} \right), \tag{A11}$$

where $\gamma = E_s(s^2)/2\sigma_N^2 = \exp(2\mu_s + 2\sigma_s^2)/2\sigma_N^2$ is the mean input SNR. The relationship between the detection probability and the false alarm probability is given by

$$p_D = Q\left(\frac{Q^{-1}(P_{\mathrm{FA}}) - \gamma\sqrt{N_s}}{\sqrt{[1+2\gamma+\gamma^2(\exp(4\sigma_s^2)-1)]}} \right). \tag{A12}$$

[1] J. G. Proakis, *Digital Communications* (McGraw-Hill, New York, 2001).
[2] M. Stojanovic, J. G. Proakis, J. A. Rice, and M. D. Green, "Spread spectrum underwater acoustic telemetry," Proceedings of MTS/IEEE OCEANS '98, 1998, Vol. **2**, pp. 650–654.
[3] E. M. Sozer, J. G. Proakis, M. Stojanovic, J. A. Rice, A. Benson, and M. Hatch, "Direct sequence spread spectrum based modem for under water acoustic communication and channel measurements," Proceedings of MTS/IEEE OCEANS '99, 1999, Vol. **1**, pp. 228–233.
[4] G. D. Weeks, J. K. Townsend, and J. A. Freebersyser, "A method and metric for quantitatively defining low probability of detection," IEEE Military Communication Conference Proceedings, 1998, Vol. **3**, pp. 821–826.
[5] H. Urkowitz, "Energy detection of unknown deterministic signals," Proc. IEEE **55**, 523–531 (1967).
[6] M. Stojanovic and L. Freitag, "Hypothesis-feedback equalization for direct-sequence spread-spectrum underwater communications," Proceedings of MTS/IEEE OCEANS '00, 2000, Vol. **1**, pp. 123–129.
[7] F. Blackmon, E. M. Sozer, M. Stojanovic, and J. Proakis, "Performance comparison of RAKE and hypothesis feedback direct sequence spread spectrum techniques for underwater communication applications," Proceedings of MTS/IEEE OCEANS '02, 2002, Vol. **1**, pp. 594–603.
[8] M. Stojanovic and L. Freitag, "MMSE acquisition of DSSS acoustic communications signals," Proceedings of MTS/IEEE Oceans '04, 2004, Vol. **1**, pp. 14–19.
[9] T. C. Yang and W.-B. Yang, "Low signal-to-noise-ratio underwater acoustic communications using direct-sequence spread-spectrum signals," Proceedings of OCEANS 2007, Aberdeen, UK, 2007.
[10] T. C. Yang and W.-B. Yang, "Performance analysis of direct-sequence spread-spectrum underwater acoustic communications with low signal-to-noise-ratio input signals," J. Acoust. Soc. Am. **123**, 842–855 (2008). The cross-correlation method was introduced in this paper using the concept of time-updated passive-phase conjugation. Channel estimation is not required in actual implementation.

[11]T. C. Yang, "Temporal fluctuations of broadband channel impulse functions and underwater acoustic communications at 2–5 kHz," Proceedings of IEEE/MTS OCEANS 2002, Biloxi, Oct. 2002, Vol. **4**, pp. 2395–2400.
[12]R. A. Iltis and A. W. Fuxjaeger, "A digital DS spread-spectrum receiver with joint channel and Doppler shift estimation," IEEE Trans. Commun. **39**, 1255–1267 (1991).
[13]T. C. Yang, "Measurements of temporal coherence of sound transmissions through shallow water," J. Acoust. Soc. Am. **120**, 2595–2614 (2006).
[14]B. Sklar, *Digital Communications: Fundamentals and Applications* (Prentice-Hall, Englewood Cliffs, NJ, 1988), Chap. 3, Sec. 7.
[15]J. H. Park, Jr., "LPI techniques in the underwater acoustic channel," Proceedings of IEEE Military Communication Conference, 1986, Vol. **1**, pp. 10.5.1–10.5.5.
[16]D. G. Woodring, "Performance of optimum and suboptimum detectors for spread spectrum waveforms," Naval Research Laboratory Report No. 8432, Washington, DC (1980).
[17]M. D. Collins, "A higher-order parabolic equation for wave propagation in an ocean overlying an elastic bottom," J. Acoust. Soc. Am. **86**, 1459–1464 (1989).
[18]R. J. Urick, *Principles of Underwater Sound* (McGraw-Hill, New York, 1983).
[19]R. Coates, *Underwater Acoustic Systems* (Wiley, New York, 1989).